Boundary-Layer Meteorology (2023) 187:311–338
https://doi.org/10.1007/s10546-022-00751-4

RESEARCH ARTICLE

Relationships Between Second and Third Moments in the Surface Layer Under Different Stratification over Grassland and Urban Landscapes

Kirill Barskov[1] · Dmitry Chechin[1] · Ilya Drozd[1,2] · Arseniy Artamonov[1] · Artyom Pashkin[1] · Alexander Gavrikov[1,3] · Mikhail Varentsov[1,2,4] · Victor Stepanenko[1,2,4] · Irina Repina[1,2,4]

Received: 5 February 2022 / Accepted: 19 September 2022 / Published online: 5 December 2022

Abstract
We present results from the multi-level mast eddy-covariance measurements conducted over flat grassland and over complex urban terrain composed of trees and small buildings. Relationships between the stability parameter and turbulent statistical properties were analysed. Over flat grassland, non-dimensional turbulent moments up to the third-order obey Monin–Obukhov similarity theory. Third-order moments increase for increasing instability, indicating nonlocal turbulent transport of heat flux due to convective motions, and in this case, the relationship between the third- and second-order moments obtained using the framework of the mass-flux approach might be applicable. In stable conditions, the turbulent transport of heat flux is positive and does not demonstrate an explicit dependence on stability but might be associated with large eddies and sweep motions transporting downwards the heat flux originating near the top of a stable boundary layer. Such a downward transport of negative heat flux by large eddies makes applicable the mass-flux approach even in stable boundary layers at higher levels. Over the urban landscape, for all wind directions the third moment corresponds well with the theoretical curve in cases of stable and unstable stratification, but there is a wide spread of data in near-neutral conditions. Skewness of the vertical velocity component is negative over the urban landscape and its value depends on wind direction. At lower levels, the standard deviation of the vertical velocity component is increasing with stability faster than expected from the theoretical curve. Over the urban landscape, large roughness elements do not affect the performance of the mass-flux approach in the convective boundary layer. Furthermore, there is a link between the second and third moments even in stable boundary layers over heterogeneous landscape.

✉ Kirill Barskov
barskov@ifaran.ru; barskovkv@gmail.com

1 A. M. Obukhov Institute of Atmospheric Physics RAS, Moscow, Russia 119017

2 Research Computing Center, Moscow State University, Moscow, Russia 119234

3 P. P. Shirshov Institute of Oceanology RAS, Moscow, Russia 117218

4 Moscow Center for Fundamental and Applied Mathematics, Moscow, Russia 119234

Keywords High-order moments · Inhomogeneous surface · Monin · Obukhov similarity theory · Skewness · Turbulence

1 Introduction

Estimating the momentum, heat and mass exchange between the atmosphere and underlying surface is an important part of atmospheric boundary-layer research. The traditional parametrizations used in atmospheric modelling are based on Monin–Obukhov similarity theory (MOST) (Monin and Obukhov 1954), which assumes horizontal homogeneity of the underlying surface as well as statistical stationarity of a turbulent flow (Monin and Yaglom 1992). The MOST approach has been experimentally verified for homogeneous surfaces (e.g. Mordukhovich and Tsvang 1966; Izumi 1971; Tsvang et al. 1973, 1985; Stull 1988; Sorbjan 1989; Kaimal and Finnigan 1994; Wyngaard 2010), while the applicability of MOST over complex and heterogeneous surfaces is still an open issue due to many difficulties when applying traditional scaling rules since MOST assumptions may not be fulfilled. In particular abrupt changes in roughness, temperature or other surface properties along an interface (such as the sea–land transition, forest edge, patchy vegetation etc.) may lead to the formation of internal boundary layers (Garratt 1990; Medjnoun et al. 2018), to an increase of the role of advection (Rao et al. 1974; Fontan et al. 2013; Higgins et al. 2013), and to the occurrence of secondary circulations (Raasch and Harbusch 2001; Fontan et al. 2013). The structure of a turbulent flow near the downwind forest edge or building may resemble the structure of a backward-facing-step flow with the formation of a recirculation zone with a quasi-two-dimensional vortex in the vertical plane (Condie and Webster 2001; Boehrer and Schultze 2008; Markfort 2010; Kenny et al. 2017). The large-eddy simulation results show that there is an intense production of turbulent kinetic energy and second turbulent moments induced by large velocity shear at the tree height in this case (Glazunov and Stepanenko 2015; Kenny et al. 2017). The problems of studying atmospheric processes over landscapes with different scales of heterogeneities, as well as the development of parametrizations of turbulent exchange over such territories in numerical weather and climate models, are widely discussed in the scientific literature (e.g., Giorgi and Avissar 1997; Ament and Simmer 2006; Bou-Zeid et al. 2004, 2020; Babić et al. 2016a,b). But, despite the progress in this area achieved in recent decades, the problems of taking into account the influence of a heterogeneous surface in weather and climate modelling are far from being satisfactorily solved. Field studies over heterogeneous surfaces including forest sites (e.g. Nakamura and Mahrt 2001; Dellwik and Jensen 2005; Barskov et al. 2018), urban areas (e.g. Quan and Hu 2009; Wood et al. 2010), forest lakes (Barskov et al. 2017, 2019; Ala-Könni et al. 2021), sea ice (e.g. Rodrigo and Anderson 2013; Grachev et al. 2013, 2015; Michaelis et al. 2020), and coastal zones (Soloviev and Kudryavtsev 2010; Zhao et al. 2013; Kral et al. 2014; Grachev et al. 2018) show that MOST may be applicable, but it has to be extended to inhomogeneous conditions by adjusting universal functions, introducing additional scaling parameters or also taking into account wind direction.

When the characteristic scale of inhomogeneity (such as the height of buildings and canopy) is comparable to or even larger than the measurement level, the turbulent transport can be carried out by eddy motions, whose size is larger than the scale at which the mean gradients change. As a result, local MOST scaling may fail, and large eddies have to be accounted for in the turbulence closures. In particular counter-gradient transport of heat and water vapor can exist in the vegetation canopy (Denmead and Bradley 1985). One of the

reasons is the vertical turbulent transport carried out by organized eddy motions (Finnigan 2000; Dupont and Brunet 2009; Katul et al 2013; Banerjee et al 2017).

The important role of mixing due to large eddies was especially well studied for the convective boundary layer (CBL). Within the CBL, the turbulent vertical velocity probability density function has positive skewness indicating that strong narrow updrafts are surrounded by larger areas of weaker downdraft (Moeng and Rotunno 1990). Zilitinkevich et al. (2021) proposed that buoyancy produces chaotic vertical plumes that merge into larger ones and produce an inverse cascade resulting in their transition to self-organized regular motions. Zilitinkevich et al. (1998, 2006) showed that in the CBL close to the surface large coherent eddies cause convergent winds, which in turn cause wind shears and the generation of turbulence. This mechanism strongly enhances the convective heat/mass transfer at the surface and implies an important role of the surface roughness, which may be especially important over inhomogeneous landscape. For convective conditions, several approaches of different levels of complexity have been proposed in order to parametrize the nonlocal mixing due to large eddies. For example, the "mass-flux" and "bottom-up-top-down" approaches make it possible to close the system of equations for the second moments in the atmospheric boundary layer (Abdella and McFarlane 1997, 1999; Zilitinkevich et al. 1999; Abdella and Petersen 2000; Mironov et al. 1999, 2000; Gryanik and Hartmann 2002; Ferrero 2005). One can assume that this theoretical formalism should be valid for any boundary layer (Zilitinkevich 2002) in which the vast majority of the dispersion of hydrodynamic fields is carried out by organized structures including also the atmospheric flow over a geometrically complex surface.

Large-scale organized eddy motion affects the statistical probability distribution of scalars. High-order moments reflect to a certain extent the characteristics of the probability density of the lower-order moments (Lyu et al. 2018), which is why investigating high-order moments is necessary over complex terrain. For example, skewness is associated with the asymmetry of the distribution with respect to its mean and it is considered to have relevance for nonlocal transport (Quan et al. 2012). Earlier we showed (Barskov et al. 2019) that third-order moments are responsible for the nonlocal turbulent transport caused by a heterogeneity of landscape.

At the same time, in the surface layer MOST is used. Obviously, a correct and careful matching between MOST and higher-order closures is needed in order to provide adequate boundary conditions for the boundary-layer parametrizations. This is yet another reason why it is important to consider the behaviour of higher-order moments in the surface and boundary layers over various landscapes.

The goals of this study are (i) to document the performance of the classical MOST scaling over surfaces with a different level of heterogeneity and (ii) to consider the behaviour of the third-order moments such as the vertical velocity skewness and the turbulent transport of a scalar flux. In particular, a homogeneous grassland landscape and an urban landscape. Both stable and unstable stratification are considered. Turbulence moments are investigated as functions of the stability parameter and are compared with the well-established universal functions. The deviations from the latter are considered as possible hints to the effect of landscape heterogeneities. The special focus is on a relation between the third moment, namely, the turbulent transport of a kinematic heat flux, vertical velocity skewness and heat flux. Such a strategy follows from our earlier study (Barskov et al. 2019), where it was shown that, during episodes with a strong temperature inversion in the atmospheric boundary layer, the local heat flux over a flat surface surrounded by forest was produced by turbulent transport from aloft rather than by local gradients of wind speed and temperature. In such conditions, local MOST scaling failed. Instead, observations suggested that the approaches developed earlier to parametrize nonlocal transport in mixed layers using vertical velocity skewness and second-order moments might be applicable.

The paper is organized as follows. In Sect. 2, an overview of classical similarity functions describing various turbulence moments as functions of the stability parameter is given with a focus on the vertical velocity variance, skewness and the turbulent transport of scalars. In the last part of Sect. 2 an overview of deviations of these turbulent moments from classical similarity functions in the atmospheric boundary layer (ABL) in the case of inhomogeneous landscape is given. In Sect. 3, two observational sites in contrasting landscapes as well as methods are described. In Sect. 4, the observed dependencies of the considered turbulence moments on the stability parameter is presented and the agreement/disagreement with classical universal functions is highlighted. In Sect. 5, the obtained results are summarized and the possible effects of landscape heterogeneities are discussed.

2 Relationships Between Second and Third Moments

In this study$u$, v and w are the longitudinal, lateral and vertical velocity components, T is the air temperature while θ_v is the virtual potential temperature. The turbulent fluctuations are computed following $x' = x - \overline{x}$, where x is any variable, the overbar denotes the time averaging operator, and the primed variable denotes the turbulent part. Time is denoted as t.

As stated in the Introduction, the focus of this study is on turbulent transport of scalars. In the following, we consider the rate equation for the turbulent heat flux in order to establish a diagnostic framework which, alongside with MOST, will be used for the data analysis. The evolution of the vertical heat flux is governed by:

$$\underbrace{\frac{\partial \overline{w'\theta_V'}}{\partial t}}_{I} = \underbrace{-\overline{w'u_k'}\frac{\partial \overline{\theta_v}}{\partial x_k}}_{II} \underbrace{-\overline{u_k}\frac{\partial \overline{\theta_v' w'}}{\partial x_k}}_{III} \underbrace{-\overline{\theta_v' u_k'}\frac{\partial \overline{w}}{\partial x_k}}_{IV} \underbrace{-\frac{\partial \overline{u_k' w'\theta_v'}}{\partial x_k}}_{V}$$
$$\underbrace{+\overline{w'\kappa_T \nabla^2 \theta_v'} + \overline{\theta_v' \vartheta \nabla^2 w}}_{VI} \underbrace{-\frac{1}{\rho_0}\overline{\theta_v'\frac{\partial p'}{\partial z}}}_{VII} + \underbrace{\frac{g}{T_0}\overline{\theta_v'^2}}_{VIII}, \tag{1}$$

where κ_T is thermal diffusivity coefficient, ϑ is kinematic air viscosity, ρ_0 is air density, p is air pressure, and g is the acceleration due to gravity. Here, Einstein summation notation is assumed. The left-hand side is the heat-flux tendency (I), and right-hand side terms are, in order, production by the temperature gradient (II), the temperature flux advection (III), the vertical wind shear production (IV), the third-moment turbulent transport (V), dissipation (VI), the pressure production (VII), and the buoyancy generation (VIII). This equation contains third moments in term (V) that represent vertical and horizontal transports of the heat flux. The third moments which represent horizontal transport of fluxes are assumed to be zero over horizontally homogeneous surface, and the third moment $\overline{w'w'\theta_v'}$ represents the vertical turbulent flux of heat flux.

The Monin–Obukhov stability parameter is defined as the ratio of measurement level z to the Obukhov length scale L (Obukhov 1946),

$$\zeta = \frac{z}{L} = -\frac{z\kappa g \overline{w'\theta_v'}}{u_*^3 \theta_v}, \tag{2}$$

where $\kappa = 0.4$ is the von Kármán constant, and $u_* = \left(\overline{u'w'}^2 + \overline{v'w'}^2\right)^{1/4}$ is the friction velocity. The traditional sign convention for the Monin–Obukhov stability parameter is used, where $\zeta > 0$ corresponds to a stable boundary layer, and $\zeta < 0$ represents a CBL. It is

important to note that everywhere in this study we are considering turbulence moments which contain the fluctuations of acoustic temperature T'_{soinc} rather than of physical air temperature T'. This is convenient, as acoustic temperature closely approximates the virtual air temperature T_v. The fluctuations of the latter $T_v^{'}$ are related to the buyoancy flux and are used in the definition of the Obukhov length L. For simplicity, we use T' instead of $T_v^{'}$ or T'_{sonic} everywhere in the following. The temperature scale is $T_* = \overline{w'T'}/u_*$. In our notation T_* has the same sign as $\overline{w'T'}$ and the opposite sign as L, it is convenient for normalizing the third moment using T_*.

2.1 Unstable Stratification

In the CBL the transport of the third-order moments contributes significantly to the rate Eq. (1) of the second moment. Zilitinkevich et al. (1999) demonstrated that it is the third-order moment $\overline{w'w'T'}$ that is largely responsible for the nonlocal nature of turbulent transport in a CBL. According to a bimodal bottom-up–top-down model (Zilitinkevich et al. 1999) and the mass-flux model (Abdella and McFarlane 1997) in an idealized convective circulation composed of rising and sinking branches, updrafts, and downdrafts, the vertical turbulent advection of the heat flux $\overline{w'w'T'}$ is proportional the to heat flux $\overline{w'T'}$, with the proportionality coefficient including the skewness of vertical velocity $S_w = \overline{w'w'w'}/\left(\overline{w'w'}\right)^{3/2}$:

$$\overline{w'w'T'} = C S_w \left(\overline{w'w'}\right)^{1/2} \overline{w'T'}, \tag{3}$$

where C is a dimensionless constant of order 1. In parametrization (3), the term $S_w\left(\overline{w'w'}\right)^{1/2}$ was called by Zilitinkevich et al. (1999) the "large-eddy skewed-turbulence advection velocity". As noted by Zilitinkevich et al. (1999), Eq. (3) is valid in the well-mixed part of the boundary layer, where the vertical temperature gradient is close to zero. For more stratified regions of the ABL, (3) can be generalized by inclusion of the downgradient diffusion term (Eq. (24) in Zilitinkevich et al. 1999). For further analysis, we rewrite Eq. (3) in dimensionless form with u_* and T_* and obtain:

$$\frac{\overline{w'w'T'}}{u_* u_* T_*} = C S_w \frac{\sigma_w}{u_*}, \tag{4}$$

where $\sigma_w = \overline{w'w'}^{1/2}$.

In order to evaluate (4) using observations in the surface layer, let us first consider the asymptotics of various quantities in (4) in the free-convection limit assuming MOST scaling.

The asymptotic value of the third moment for free convection can be estimated as:

$$\frac{\overline{w'w'T'}}{u_* u_* T_*} \approx A_1 (-\zeta)^{1/3}, \tag{5}$$

where $A_1 \approx 1.25 - 1.30$ is the empirical constant (Wyngaard et al. 1971).

According to similarity theory S_w is positive for $\zeta < 0$ and tends to constant with increase of instability $\zeta \to -\infty$ (Monin and Yaglom 1971). A wind tunnel experiment showed that the asymptotic value of skewness for free convection is $S_w \simeq 0.33$ (Maurizi and Tampieri 2013). Field experiments give similar results: Chiba (1978) accumulated observational data and derived an empirical formula for the relationship between S_w and the stability for $\zeta \leq 0$ as:

$$S_w = -\frac{0.6\zeta}{(1.25)^3\kappa\left[(1-15\zeta)^{-\frac{1}{4}} - 1.8\zeta\right]} + 0.1. \tag{6}$$

The limit of S_w as $\zeta \to -\infty$ is $S_w = 0.53$. Taking into account uncertainty and scattering of data, one can assume that the asymptotic value of skewness for free convection $S_w = B_1 \simeq 0.3 - 0.5$.

As for the standard deviation of the vertical velocity component, according to Panofsky et al. (1977), Hicks (1981), Kaimal and Finnigan (1994), and summarized by Foken (2017), the second moment as a function of stability parameter can be estimated as:

$$\frac{\sigma_w}{u_*} = C_1(1-3\zeta)^{1/3}, \tag{7}$$

where $C_1 = 1.25 - 1.30$. The value of C_1 can be also estimated as the value of σ_w/u_* in near-neutral unstable conditions and takes a value of $C_1 = 1.25-1.45$ (Lumley and Panofsky 1964; Panofsky and Dutton 1984; McBean 1971; Foken et al. 1991). Thus one can expect $\overline{w'w'T'}/u_*u_*T_* \to A_1(-\zeta)^{1/3}$, $S_w \to B_1$, $\frac{\sigma_w}{u_*} \to C_1 3^{1/3}(-\zeta)^{1/3}$ for $\zeta \to -\infty$, which it leads to Eq. (4) with the dimensionless constant C from (4) as $C = A_1/3^{1/3}B_1C_1 \cong 1.2-2.4$.

2.2 Neutral and Stable Stratification

In weakly stable conditions, the gradient transport theory or K-theory of turbulence involves representing turbulent moments as being entirely due to down-gradient diffusion (Stull 1988: p. 204). The transport of the third-order moments in (2) is relatively small in this case, and the third moment $\overline{w'w'T'}/u_*u_*T_*$ is constant close to zero (Wyngaard et al. 1971). All the turbulent moments take constant values which depend only on u_* and T_*, in particular:

$$\frac{\overline{w'w'T'}}{u_*u_*T_*} = A_2, \tag{8}$$

$$S_w = B_2, \tag{9}$$

$$\frac{\sigma_w}{u_*} = C_2, \tag{10}$$

where $A_2 \approx 0.55$ (Kader and Yaglom 1990), $C_2 \approx 1.25 - 1.50$ (Ariel and Nadezhina 1977; Caughey et al. 1979; Kader and Yaglom 1990; De Bruin et al. 1993). The value of B_2 can be estimated as a limit of S_w from (6) with $\zeta \to 0$: $S_w \to 0.1$. According to Maurizi and Robins (2000), within the surface-layer skewness of the vertical component of velocity in neutral conditions is nearly constant at $S_w \simeq 0.05$. So one can estimate $B_2 = 0.05 - 0.10$. This parametrization, however, fails when larger-size eddies are present in the flow.

As stable stratification sets in and becomes stronger, it inhibits vertical motions and the turbulence no longer communicates significantly with the surface (Monin and Yaglom 1971), so the distance z to the surface no longer plays any role in the structure of turbulence. That is, various quantities become independent of z, the so-called "z-less stratification" (Wyngaard 1973), leading to all scaled turbulent statistics being either constant or linear with ζ (Dias et al. 1995). In particular, the standard deviation of the vertical velocity component as a function of stability parameter can be estimated as:

$$\frac{\sigma_w}{u_*} = C_3(1+0.2\zeta) \tag{11}$$

where $C_3 = 1.25$ (Kaimal and Finnigan 1994). As for $\overline{w'w'T'}/u_*u_*T_*$, Dias et al. (1995) found that the normalized third-order moment $\overline{w'w'T'}/u_*u_*T_*$ remains constant close to zero in the range $0 < \zeta < 1$, but there is a small general trend of increasing $\overline{w'w'T'}/u_*u_*T_*$ with an increase of stability which is, however, the same order as the scatter of the data (Dias et al. 1995, Fig. 3). The skewness of the vertical velocity component S_w should be smaller in stable conditions in comparison with the unstable case. According to similarity theory S_w must approach a constant value with an increase of stability $\zeta \to \infty$ (Monin and Yaglom 1971). According to Wyngaard (1973), the skewness S_w in stable conditions is constant$S_w \approx 0.1$. It however doesn't agree with the observed data (Chiba 1978), which shows a large scatter of S_w between -0.4 and 0.2 for $\zeta > 0$ with a general trend of an increasing negative value of S_w with increasingζ.

Under very stable conditions, the so-called "supercritical regime", the inertial subrange associated with the Richardson–Kolmogorov cascade dies out, and vertical turbulent fluxes become small with the inclusion of non-turbulent motions (Grachev et al. 2013). Thus, the data in the region $\zeta \gg 1$ may be beyond the limits of applicability of similarity theory (Babić et al. 2016a) and σ_w/u_* becomes smaller than described by the linear form (11) in these periods (Grachev et al. 2013).

2.3 Influence of the Surface Heterogeneity

All of the similarity functions mentioned above were obtained and are valid for stationary atmospheric turbulence over a homogeneous surface. Applicability of MOST over complex and heterogeneous surfaces may depend on the type of inhomogeneity. For example, equations for σ_w/u_* are applicable over terrain with metre-scale heterogeneity, such as patchy vegetation in sandy soil (Andreas et al. 1998). Research in coastal zones (Grachev et al. 2018) showed that non-dimensional standard deviations generally also obey Monin–Obukhov similarity theory within experimental uncertainty, but in some locations near the shoreline, σ_w/u_* collapses better onto a single universal curve for onshore than for offshore flow, where the measured σ_w/u_* is larger than predicted values. Significant differences can be found when these expressions are extrapolated to other more complex surfaces. Göckede et al. (2004) has shown degradation of the data quality of fluxes when measurements are made over heterogeneous surfaces contained within the footprint region, when compared against data collected over homogeneous surfaces. At the same time, the footprint area depends on wind direction as well as on stratification. Foken and Leclerc (2004) showed that there is a good agreement between data and the parametrized values of σ_w/u_* over heterogeneous landscape under unstable stratification. In contrast, in stable conditions a significant difference was found, and this difference depends on wind direction. In this case the source area of the flux becomes larger and includes significant heterogeneity, which produce significant mechanical turbulence. Babic et al. (2016a) investigated the stable atmospheric boundary layer over a heterogeneous surface influenced by mixed agricultural, industrial and forest surfaces. For neutral conditions, values of non-dimensional velocity variances were found to be smaller at the lowest measurement level and larger at higher levels in comparison to classical values found over flat terrain. The ratio of the observed dimensionless standard deviation of the vertical wind component and of the theoretical one for flat and homogeneous terrain shows considerable variation with wind direction.

According to field and wind tunnel experiments for various canopy types, height, area index and foliage distribution (Wilson and Shaw 1977; Raupach et al. 1986; summarized by Raupach 1989 and Cava et al. 2006) and large-eddy simulations (Finnigan et al. 2009;

Banerjee et al. 2017), σ_w/u_* above all canopies varies little, though it has a tendency to increase with height$z$, from a value of 1.1 at level of the canopy top to a typical surface-layer value of 1.25 when z is several times larger than the canopy height. Within the canopy, σ_w/u_* is decreasing rapidly as z decreases and the turbulence is quite inhomogeneous. At the same time, the skewness S_w shifts to negative values of about $S_w \sim -0.5 \cdots -1$ within the canopy and has a positive value around $S_w \sim 0.6$ above the canopy (Seginer et al. 1976; Patton et al. 2016; Banerjee et al. 2017). As instability increases, S_w becomes larger with the same shape of profile. The opposite sign of a nonzero skewness indicates the importance of sweeps and ejections inside and above the canopy. The connection to sweep–ejection cycles and the local turbulent flux can be established through the turbulence triple moment (Poggi et al. 2004; Banerjee et al. 2017). In particular, $\overline{w'w'T'}$ is close to zero within the canopy, slightly negative near the top of the canopy and tends to be a positive constant above the canopy. Cava et al. (2006) showed that in the lower part of canopy, the normalized triple moment $\overline{w'w'T'}/u_*u_*T_*$ is close to zero in unstable and strongly stable conditions, while it increases with height in weakly stable conditions. At the same time $\overline{w'w'T'}/u_*u_*T_*$ has positive values about 1 near the top of the canopy in weakly and strongly stable conditions, while $\overline{w'w'T'}/u_*u_*T_*$ has negative values about -0.5 near the top of the canopy in unstable conditions.

Thus, the transport of the third-order moments over inhomogeneous landscape could contribute significantly to the rate equations of the second moments even in neutral or stable conditions. Equation 3 may be applicable in this case because of large eddies and coherent structures, but all terms may depend not only on ζ, but also on other scales associated with the scales of the landscape inhomogeneities.

3 Data and Methods

3.1 Sites and Measurements

The observations used in this study were obtained in the two similar boundary-layer experiments over grassland and over urban terrain. The first experiment was carried out in Tsimlyansk (47.6570 N, 42.0799 E) located in the south of the European part of Russia. A 30-m mast was installed over flat and uniform grassland. Two experimental campaigns took place in the period between 6 August 2020 and 14 August 2020 and between 4 August 2021 and 15 August 2021. Temperature fluctuations and three velocity components were measured using WindMaster three-dimensional Anemometers (Gill Instruments, UK) at 2 m, 10 m and 30 m levels with a 20 Hz frequency.

Another experiment was carried out in Moscow at the Meteorological Observatory of the Moscow State University (MSU, 55.7072 N, 37.5227E). The 21-m mast was installed at the clearing surrounded by different types of urban landscape including forested patches and buildings (red circle in Fig. 1d). Temperature fluctuations and three velocity components were measured using Metek uSonic-3 Scientific (formerly: USA-1) anemometers at 2 m and 10 m levels, a Metek uSonic-3 Class A anemometer at a 19 m level with a 20 Hz frequency. The level of 19 m was located above the tops of the trees in the vicinity of the mast. Six months (from November 2019 to May 2020) of data was analyzed.

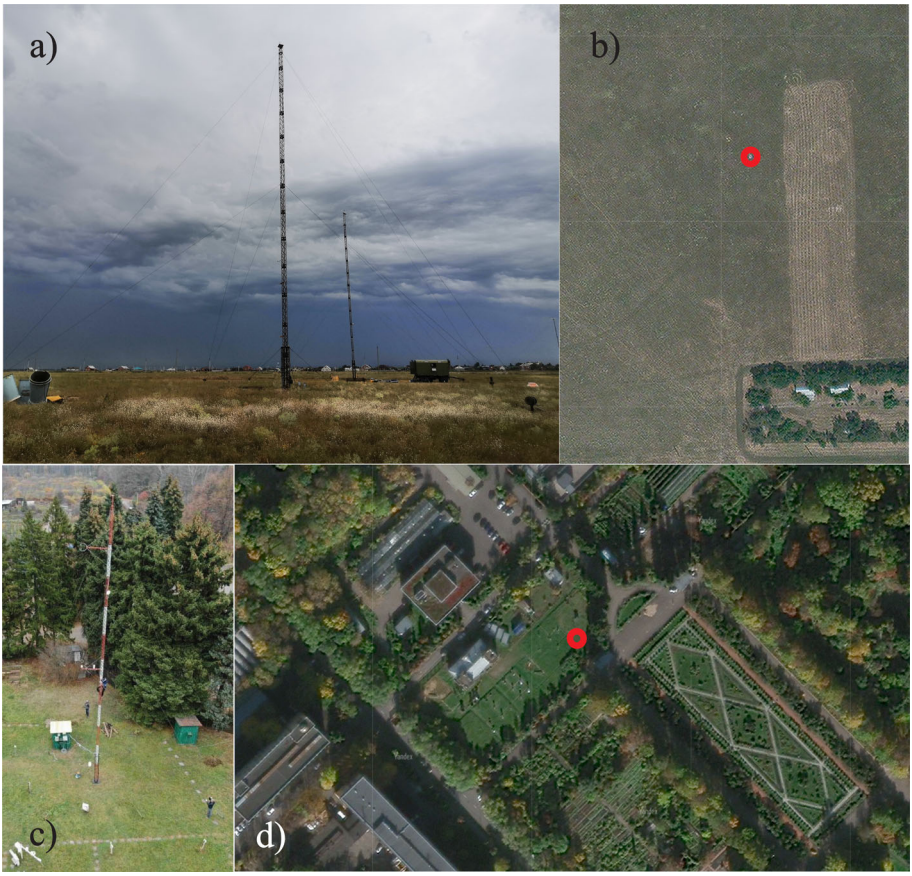

Fig. 1 View of the (**a**, **b**) Tsimlyansk mast, and (**c**, **d**) MSU mast. Photo credit: E.Shishov, M. Varentsov

3.2 Data Processing

Data preprocessing included the despiking, two-dimensional coordinate rotation for the wind components and linear detrending. Periods of mean wind speed larger than 30 m s^{-1} were removed. In the second experiment (MSU mast), periods with different wind directions were analyzed separately. Several ranges of wind directions were selected corresponding to footprint areas in specific types of urban landscape (see Fig. 4 for details). The Monin–Obukhov stability parameterζ, friction velocityu_*, and temperature scale T_* were estimated based on the turbulent fluxes measured at each observational level (local scaling). Both stable and unstable stratifications were observed in all experiments, but time intervals with $|\zeta| < 0.005$ were not included in analysis since small values of T_* in these cases lead to a large scatter of $\overline{w'w'T'}/u_*u_*T_*$. We also selected only the intervals with stationary turbulence to be confident that the time averaging is equivalent to ensemble averaging. For this purpose, we used the criterion proposed by Foken and Wichura (1996) for each second- and third-order moment. Only those periods that passed all tests for all turbulent moments were left for the analysis.

3.3 Analysis of Turbulent Moments

For further analysis of a relationship between $\overline{w'w'T'}/u_*u_*T_*$ and $S_w\ \sigma_w/u_*$ we investigated the applicability of Eq. (3). The constant C was determined as a slope of a linear regression between the observed value of the considered moments. The coefficient of determination R^2 was used as a criterion of general applicability of Eq. (4). For estimating the scatter of data, we introduce the parameter of relative scattering RS as a root-mean-square error between data y and linear approximation $\widehat{y}$ normalized by the range of the measured data along the x-axis:

$$RS = \frac{1}{x_{\max} - x_{\min}} \sqrt{\frac{\sum_{n=1}^{N} (\widehat{y_n} - y_n)^2}{N}}. \tag{12}$$

The parameter RS in this definition can be interpreted as the "width" of the distribution in comparison with its "length". The value of RS is zero when all data collapse onto a line regardless of slope and the value of RS increases when the scatter increases. The normalized root-mean-square error is sometimes used as a scatter index for model verification (e.g. Ris et al 1999).

Equation (4) may contain self-correlation (Hicks 1978) since both $\overline{w'w'T'}/u_*u_*T_*$ and $S_w\ \sigma_w/u_*$ depend on u_*. To test the role of self-correlation in our dataset we followed the approach of randomizing data by randomly shuffling the variables as described in Klipp and Mahrt (2004), Sodemann and Foken (2004), Babić et al. (2016a). Random datasets were created by redistributing the values of $\overline{w'w'T'}$, $\overline{w'w'w'}$, $\overline{w'T'}$, $\overline{w'w'}$ and u_* from the original datasets separately for $\zeta > 0$ and $\zeta < 0$. We repeated this process 1000 times and then calculated corresponding 1000 random coefficients of determination between $\overline{w'w'T'}/u_*u_*T_*$ and $S_w\ \sigma_w/u_*$ as well as slope C and scattering RS of data. The average of these 1000 random coefficients of determination R^2_{rand}, slopes C_{rand} and relative scattering RS_{rand} as well as the standard deviation of these values from the average in a random sample were used as a measure of self-correlation because random data no longer have any physical meaning. The results of the self-correlation assessment are showed in Sect. 4.3.

3.4 Averaging Time

The averaging time may have a significant influence on the calculated turbulence statistics, especially for high-order moments. When a short averaging time is chosen, the statistics may exclude the contributions by low frequency turbulent motions, and random sampling issues may contaminate the statistics. When a too long averaging time is chosen, the statistics may be influenced by the diurnal cycle of the fluxes (Mahrt 2010). In addition, if the length of experimental data series is limited and the averaging time is too long, the number of datapoints with fluxes decreases, and the statistical analysis of estimated fluxes becomes less reliable. The sampling time depends on the atmospheric stratification, wind velocity, and the measurement height. For second moments for heights of 2–5 m, 10–20 min would be required for the daytime unstable stratification (summer) and about 30–60 min and sometimes as long as 120 min for the night-time stable stratification (Foken 2017). In practice, an interval of 30 min is usually used for calculating second moments. Third-order moments, unlike second-order ones, require progressively longer and richer samples (Sreenivasan et al. 1978). Nevertheless, a 30-min interval has also been used in some studies on high-order moments of turbulent fluctuations (Jacobs et al. 2001; Lyu et al. 2018). The convergence of the obtained statistics was tested for increasing averaging interval and the value of 60 min was chosen.

4 Results and Discussion

4.1 Grassland

First, we consider results obtained over the flat grassland in Tsimlyansk. All terms of (3) as functions of ζ are shown in Fig. 2.

Under near-neutral weak unstable stratification all turbulent moments values coincide with theoretical values (Fig. 2 a, b, c). When instability increases, convective circulation composed of rising and sinking branches, updrafts, and downdrafts leads to nonlocal vertical transports of fluxes (Abdella and McFarlane 1997). The third moment $\overline{w'w'T'}/u_*u_*T_*$ increases and it agrees well with Eq. (5) (Fig. 2a, dashed line). If a is the fractional area occupied by the updrafts, the skewness S_w of the vertical velocity can be written as (Randall et al. 1992):

$$S_w = \frac{1-2a}{\sqrt{a(1-a)}}, \tag{13}$$

where turbulence in the CBL is driven by surface heating, updrafts rise much quicker and cover an area smaller than downdrafts. It leads to decreasing values of a and increasing values of S_w from the small value $S_w = B_2 = 0.05 - 0.10$ (corresponding to the a=0.48–0.49) to asymptotic value $S_w = 0.5$ (corresponding to a=0.38), as we can see at Fig. 2b. Thus, the skewness of vertical velocity S_w for $\zeta < 0$ shows a significant scatter, but generally agrees with Eq. (6) as well as with the asymptotic values of skewness 0.05 and 0.53 for neutral conditions and for free convection, respectively (Fig. 2b). The observed non-dimensional standard deviation σ_w/u_* coincides with the universal functions for unstable cases (Eq. (7), Fig. 2c). Thus, the variables $\overline{w'w'T'}/u_*u_*T_*$, S_w and σ_w/u_* increase with an increase of

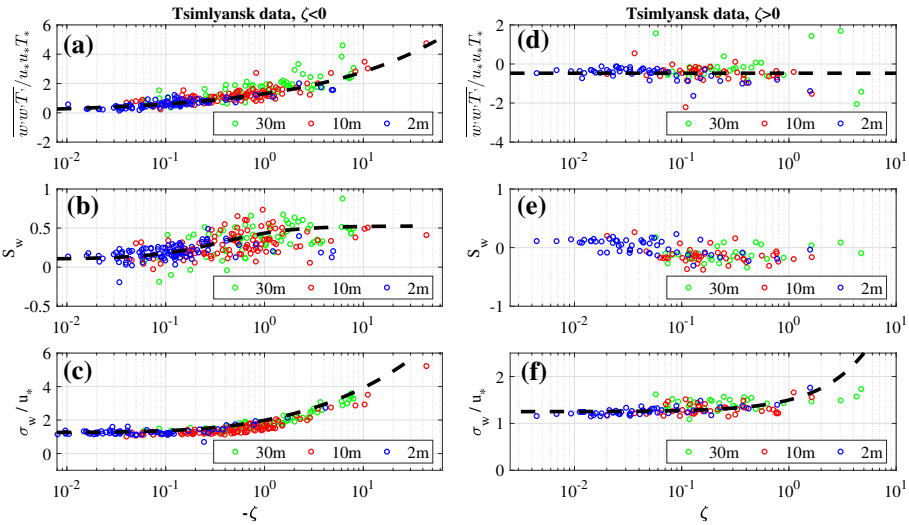

Fig. 2 Non-dimensional third-order moment $\overline{w'w'T'}$ (**a**, **d**), skewness S_w (**b**, **e**) and non-dimensional standard deviation σ_w/u_* (**c**, **f**) as functions of the Monin–Obukhov stability parameter for 30 m (green dots), 10 m (red dots) and 2 m (blue dots): (**a**, **b**, **c**) unstable ABL; (**d**, **e**, **f**) stable ABL according to the Tsimlyansk data. Dashed lines are the universal functions as described by **a** Eq. (5), **b** Eq. (6), **c** Eq. (7), **d** mean value of data ($\overline{w'w'T'}/u_*u_*T_* = -0.47$); **f** Eq. (11)

instability, so one can expect that the left-hand side of (4) $\overline{w'w'T'}/u_*u_*T_*$ would correlate well with the right-hand side of (4) $S_w\ \sigma_w/u_*$ for $\zeta < 0$.

Under stable stratification with $\zeta > 0$ the observed non-dimensional standard deviation $\frac{\sigma_w}{u_*}$ coincides with the universal functions for stable stratification (Eq. (11), Fig. 2f). The third moment $\overline{w'w'T'}/u_*u_*T_*$ under stable stratification has constant negative value $\overline{w'w'T'}/u_*u_*T_* = -0.47$, though the scattering of data increases with increasing of stability (Fig. 2d). In stable conditions $T_* < 0$, so the third moment $\overline{w'w'T'}$ is mainly has a small positive value. This mean value is close to $A_2 \approx 0.55$ in (8) for the weakly stable case, but with an opposite sign, because of the negative T_*. A positive triple correlation in stable stratification indicates possible counter gradient fluxes, i.e. fluxes which are not in agreement with the mean gradient and probably related to coherent structures. Such a turbulent transport of heat flux might be associated with large eddies and sweep motions transporting downwards the heat flux originating near the top of a stable ABL. Sodemann and Foken (2005) showed that there is frequent presence of a stable inversion layer over snow surfaces, that lead to counter-gradient fluxes. A stable boundary layer accompanied by the formation of a surface inversion layer was also observed at night periods in Tsimlyansk as well as jet flows with significant wind shear (Zaitseva et al. 2018). There, a temperature inversion and wind shear form in the course of the night which increases the negative heat flux near the top of the ABL. This can even sometimes result in a formation of a so-called "upside-down boundary layer" where the magnitude of the heat and momentum fluxes increase with height. Such a phenomena is known from previous studies of a nocturnal ABL (Sun et al. 2016). This mechanism is indirectly confirmed by the fact that S_w decreases with increasing stability to a small negative constant value about -0.2 (Fig. 2e), so the fractional area a occupied by the updrafts increases to 0.55, which indicates more intensive downdrafts covering a smaller area. Another indirect indicator of nonlocal transport of the heat flux under stable stratification are the relationships between $\overline{w'w'T'}/u_*u_*T_*$ and $S_w\ \sigma_w/u_*$ as for the mass-flux model. According to Tsimlyansk, values of σ_w/u_* tend to increase while S_w tends to decrease with an increase of stability, although the scatter in the data is significant. Taking into account the weak dependance $\overline{w'w'T'}/u_*u_*T_*$ on ζ, one can expect relationships between $\overline{w'w'T'}/u_*u_*T_*$ and $S_w\ \sigma_w/u_*$ even in stable stratification. This is demonstrated in Fig. 3, where the dimensionless third moment $\overline{w'w'T'}/u_*u_*T_*$ is shown as a function of the product $S_w\ \sigma_w/u_*$ and there is good correlation between $\overline{w'w'T'}/u_*u_*T_*$ and $S_w\frac{\sigma_w}{u_*}$ in stable boundary layer at levels 30 m and partly at 10 m.

Figure 3 shows a good correlation between $\overline{w'w'T'}/u_*u_*T_*$ and $S_w\ \sigma_w/u_*$ for unstable stratification at all levels (Fig. 3a, b, c). While the instability increases (colour of dots change from blue to red) all third moments increase with it. The constant C as a slope from Eq. (3) is similar at all levels and close to 2 within uncertainty. Relative scattering is the same at all levels $RS = 0.2$. At the same time the coefficient of determination R^2 increases with increasing height, likely because large eddies have maximal impact in the middle of boundary layer. So, Eq. (3) is applicable well in unstable stratification.

There is also a correlation between $\overline{w'w'T'}/u_*u_*T_*$ and $S_w\ \sigma_w/u_*$ for stable stratification at levels 30 m and 10 m, but not at 2 m (Fig. 3d, e, f). This may indicate the existence of a nonlocal transport of heat fluxes in the stable boundary layer, and this mechanism doesn't explicitly depend on the value of ζ (dot colours appear randomly distributed). The value of C is equal to 1.6 and 1.8 at levels 30 m and 10 m respectively. The value of R^2 is a bit larger at 30 m than at 10 m (0.7 in comparison with 0.6), and the relative scattering values at 30 m and 10 m are comparable with those in unstable cases. At the same time there is a weak relation between $\overline{w'w'T'}/u_*u_*T_*$ and $S_w\ \sigma_w/u_*$ at 2 m in stable conditions: when

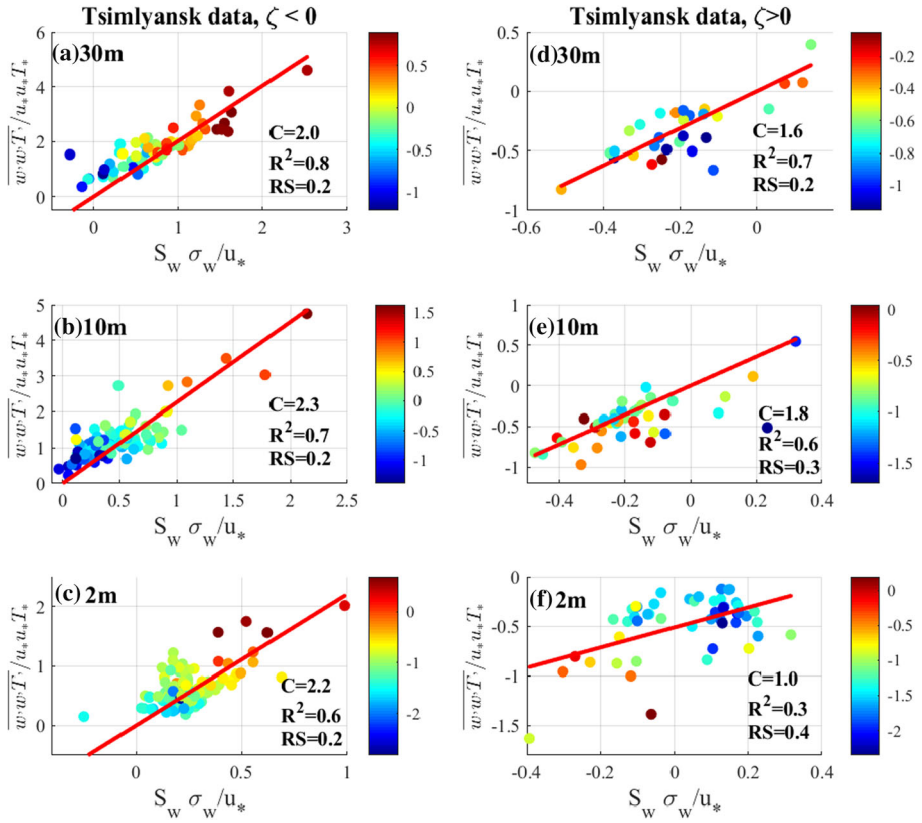

Fig. 3 Dimensionless third moment versus the product of skewness and the standard deviation for unstable (left column) and stable (right column) stratification at levels of 30 m, 10 m and 2 m according to the Tsimlyansk data. The dots denote observational data, and the red lines stand for the linear fit obtained using the least-squares method. Thereby, the slope of the line approximates the value of C from (3), R^2 is the coefficient of determination and RS is the relative scattering from (12). The colours correspond to $\log_{10}\zeta$ and $\log_{10}-\zeta$ for stable and unstable states, respectively

$S_w\ \sigma_w/u_*$ increases, $\overline{w'w'T'}/u_*u_*T_*$ generally increases too, but $R^2 = 0.3$ reveals a bad correlation, and the slope $C = 1.0$ is much less than at 10 m and 30 m, the dependence does not pass through zero, and scattering of data $RS = 0.4$ is larger than in other cases.

4.2 Complex Urban Terrain

In this subsection, the results of the urban experiment are presented. The 21-m mast at the MSU observatory was surrounded by different types of urban landscape, as shown in Fig. 4.

Since measurements were performed in a very heterogeneous landscape, normalized turbulent statistics may depend not only on the dimensionless heightζ, but also on other scales associated with the scales of the landscape inhomogeneities. These scales may depend on wind direction, and even within one particular wind direction they may depend on the footprint area (Foken and Leclerc 2004) as the latter changes depending on stratification. Figure 5 shows the normalized third-order moment $\overline{w'w'T'}$, σ_w and S_w, as well as the normalized wind

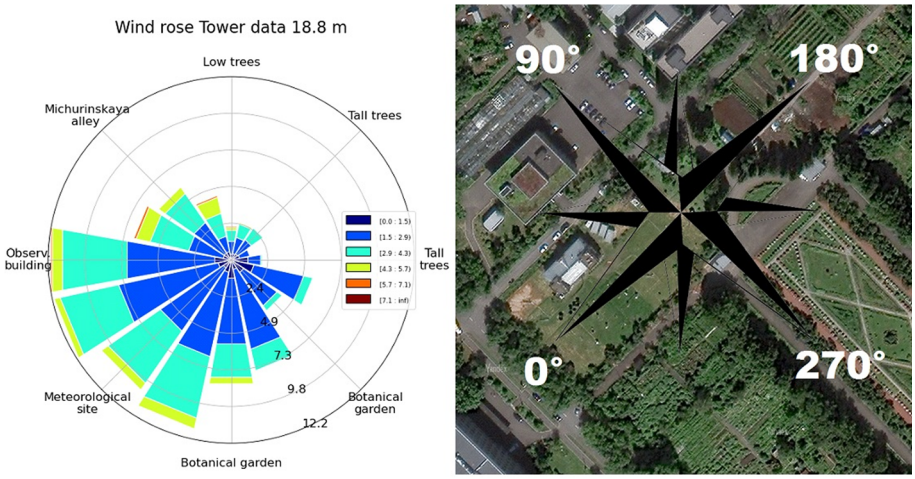

Fig. 4 Wind rose for the analysed period and the wind direction scheme

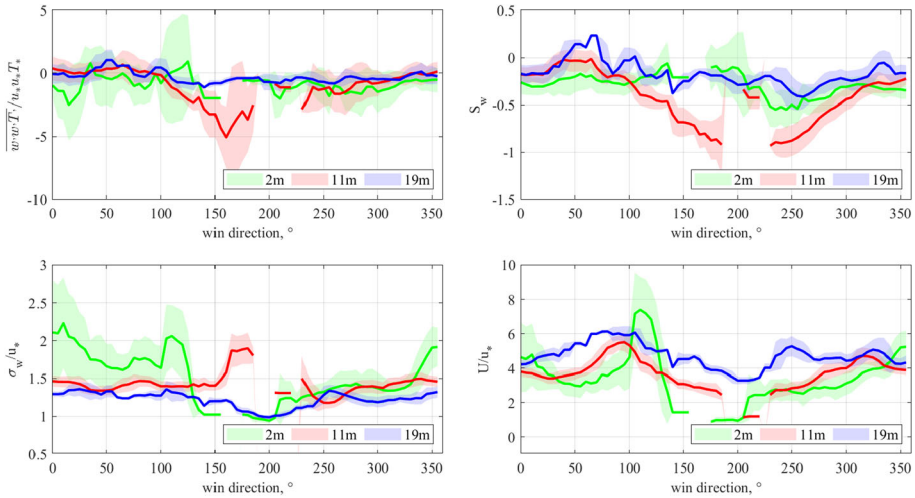

Fig. 5 Turbulent statistics under near-neutral weak stable stratification ($0.005 < \zeta < 0.05$) as functions of wind direction. Solid curves represent bin-averaged values and filled area denotes the plus/minus standard deviation

velocity $\frac{U}{u_*}$ for each observational level calculated for the near-neutral stable stratification ($0.005 < \zeta < 0.05$) as functions of wind direction.

Obviously, there is a strong dependency of the considered quantities on wind direction. Based on Fig. 5, two wind direction intervals are selected for an independent analysis, namely (i) wind direction from 0 to 100° and (ii) wind direction from 140 to 250°.

4.2.1 Wind Directions from 0 to 100°

When the wind direction is from 0 to 100° the flow first passes over a large area of the botanical garden with bushes and small trees or an urban landscape with small trees, bushes, small buildings, fence etc., and then finally over a flat clearing which has a width of 30–100 m directly upwind of the mast.

The level of 19 m is higher by more than a factor of two than all the mentioned roughness elements. At this level, the value of $\sigma_w/u_* = 1.25 - 1.35$ (Fig. 5b, blue line) is generally close to the values of C_1 in (7) and C_2 in (10) reported for the inhomogeneous surface, when the measurement level is several times higher than the heights of roughness elements: over an urban landscape with trees $\sigma_w/u_* = 1.37$ (Babic et at. 2016a), over the city $\sigma_w/u_* = 1.40$ (Wood et al. 2010), over valley with forested ridges $\sigma_w/u_* \approx 1.2$ (Moraes et al. 2005), and also according to the wind tunnel experiments $\sigma_w/u_* = 1.21$ (Raupach et al. 1986). The dimensionless wind velocity U/u_* at 19 m depends on the wind direction and has a typical value of 4–6 for tall vegetation, $\overline{w'w'T'}/u_*u_*T_*$ at 19 m is close to zero which is also in agreement with the Tsimlyansk data for neutral stratification. The value of S_w varies slightly from -0.2 to 0.2 for different wind directions.

The level of 11 m is higher but is of the same order of magnitude as the heights of roughness elements. When airflows over changing terrain, an internal boundary layer develops over the new roughness, growing in height with downwind distance. That's why the level of 11 m may be in the internal boundary layer formed during the transition from the urban landscape to the clearing around the mast, or somewhere else around. In this case at 11 m $\frac{\sigma_w}{u_*}$ increases, S_w and $\frac{U}{u_*}$ slightly decrease in comparison to 19 m. These results agree with measurements above canopy close to canopy top (Banerjee et al. 2017).

The level of 2 m is lower than the buildings heights around the clearing, but turbulent moments significantly differ from those typically reported for the canopy layer. In particular, σ_w/u_* is increased as compared to 11 m and 19 m heights and takes large values of up to 2 with large variability. In the contrast, previous studies reported a decrease of σ_w/u_* in the canopy layer (Wilson and Shaw 1977; Raupach et al. 1986; Cava et al. 2006; Finnigan et al. 2009; Banerjee et al. 2017). Third moments are also larger in magnitude at this level. In particular, S_w becomes clearly negative at this height.

The above analysis highlights the deviations of turbulence statistics from those over a homogeneous surface caused by the heterogeneities of the urban landscape under neutral conditions. In the following, the effect of stratification is considered. All terms of (3) as functions of ζ for wind direction from 0 to 100° are shown in Fig. 6.

The third-order moment $\overline{w'w'T'}/u_*u_*T_*$ in the near-neutral weak unstable case significantly differs from the theoretical curve and from the constant value of 0.55 (Fig. 5a). Namely, as ζ approaches the neutral range, $\overline{w'w'T'}/u_*u_*T_*$ becomes negative at all levels, while data over a homogeneous landscape show small yet positive values. This result agrees with $\overline{w'w'T'}/u_*u_*T_*$ within the forest canopy (Cava et al. 2006). Interestingly, as instability increases, the spread of points decreases and they collapse in a curve close to the free convection universal function especially at levels 11 m and 19 m. This suggests that the asymptotic of the free convection is applicable for the third-order moment even for a strong inhomogeneity of the underlying surface.

A similar behavior of $\overline{w'w'T'}/u_*u_*T_*$ is observed under stable conditions (Fig. 7d): the third moment is increasing with decreasing of ζ at all levels. As stability increases, the spread of points decreases, and the observations approach a close-to-zero constant value. Also, the third moment is considerably larger than over the homogeneous surface.

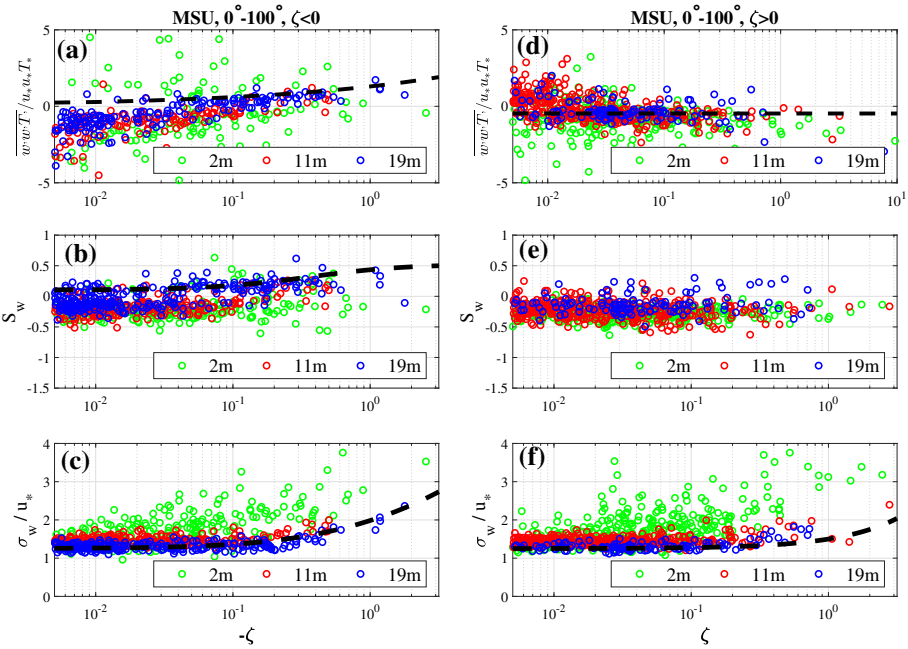

Fig. 6 Non-dimensional third-order moment $\overline{w'w'T'}$, skewness S_w and non-dimensional standard deviation σ_w/u_* as functions of the Monin–Obukhov stability parameter for 2 m (green dots), 11 m (red dots) and 19 m (blue dots): (**a**, **b**, **c**) unstable ABL; (**d**, **e**, **f**) stable ABL according to the MSU data, wind direction from 0 to 100°. Dashed lines are as for Fig. 2

As for the skewness of the vertical velocity S_w in unstable stratification, it becomes strongly negative in comparison to the data over grassland. For stable conditions, S_w is also negative.

This is in agreement with earlier observations indicating that negative skewness is typical for complex terrain (Raupach et al. 1986). The value of σ_w/u_* coincides with the theoretical curve at 19 m and strongly exceeds the theoretical curve at 2 m with significant scattering of data (Fig. 5c, f). At 11 m, σ_w/u_* demonstrates a constant shift towards higher values as compared to the theoretical curve and to the data at the 19 m level.

Thus, the data suggest that while instability increases, third moments become universal functions of ζ and the influence of heterogeneity decreases. At the same time, the standard deviation as a function of ζ has the same shape as for a flat surface but with constant shift. The applicability of Eq. (3) is discussed in Sect. 4.2.4.

4.2.2 Wind Direction from 140 to 250°

When the wind direction is from 140 to 250° the flow passes not only over the landscape with relatively small roughness elements, but also over the tall trees growing in about 10–15 m from the mast. The height of these trees is approximately 16–18 m, so that the highest measurement level is located right above the treetops. Thus, the levels 11 m and 2 m are in the lee of the high vegetation.

For these wind directions, according to Fig. 5 under near-neutral conditions, second and third moments at 19 m do not strongly deviate from their values obtained for the homogeneous

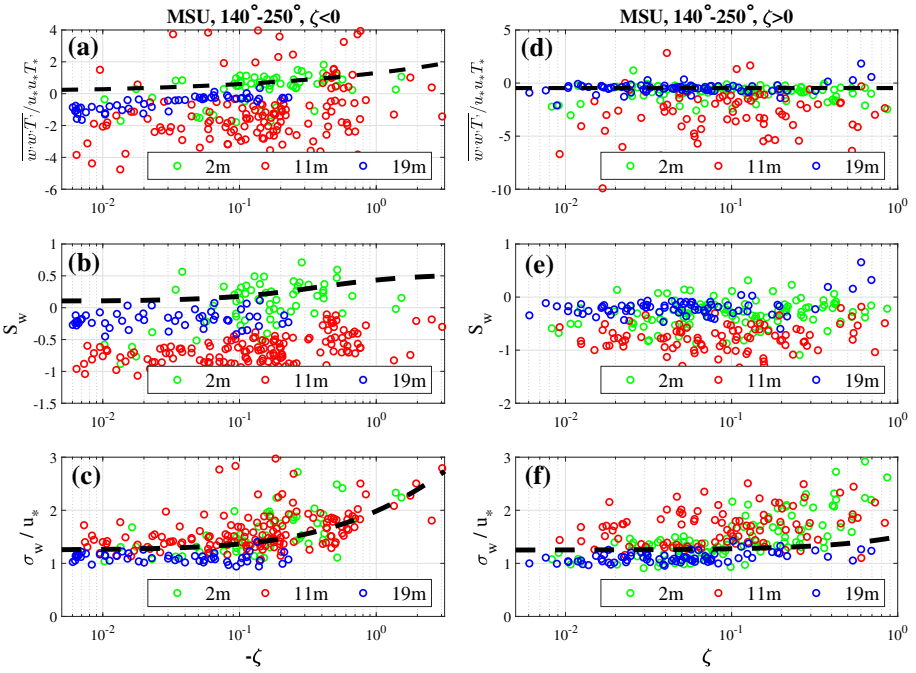

Fig. 7 Non-dimensional third-order moment $\overline{w'w'T'}$, skewness S_w and non-dimensional standard deviation σ_w/u_* as functions of the Monin–Obukhov stability parameter for 2 m (green dots), 11 m (red dots) and 19 m (blue dots): (**a**, **b**, **c**) unstable ABL; (**d**, **e**, **f**) stable ABL according to the MSU data, wind direction from 140 to 250°. Dashed lines are as for Fig. 2

case: the values of $\overline{w'w'T'}/u_*u_*T_*$ are slightly negative being close to zero, $S_w \approx -0.3$, $\sigma_w/u_* = 1.1 - 1.2$.

As for the lower two levels, the behaviour of turbulent statistics there is significantly different. The vast majority of data for this direction at 11 m and 2 m do not pass the stationarity test. The magnitude of turbulence moments at the 11 m level dramatically increases: $\overline{w'w'T'}/u_*u_*T_*$ reaches the value of -5, S_w reaches the value of -1,

σ_w/u_* increases up to 2. The scatter of the data also increases. An increase of $\overline{w'w'T'}/u_*u_*T_*$ is typical for the upper part of a canopy layer under stable stratification (Cava et al. 2006) as well as an increase of negative S_w (Raupach et al. 1986, Banerjee et al. 2017, Seginer et al. 1976). The variable σ_w/u_* also has a maxima at 11 m. It can be concluded that the height of the σ_w/u_* maxima is correlated with the height of obstacles in the upwind direction.

Note that there is lack of data with some particular wind directions at the levels 11 m and 2 m which correspond to the gaps in the curves in Fig. 5. This occurs when none of the 60-min intervals passed the stationarity test.

All terms of (3) as functions of ζ for wind direction from 140 to 250° are shown in Fig. 7.

$\overline{w'w'T'}/u_*u_*T_*$ and S_w at 11 m and 19 m shift down from the theoretical curve towards negative values in unstable stratification, being especially negative at 11 m. At the same time these are close to theoretical curves at 2 m. This result agrees well with previous measurements within a canopy (Cava et al. 2006, Raupach et al. 1986), where 11 m and 19 m correspond to the upper part of a canopy layer and 2 m is in the lower part. The behaviour of σ_w/u_* in

this case shifts down from universal function of (7) at 19 m, while at 2 m and 11 m its values are increased, especially for stable stratification. Large scattering of all turbulent statistics at 11 m indicates that they may depend on other scales within the same wind direction and stability parameter ζ.

4.2.3 Footprint

The influence of roughness elements should depend on footprint area (Foken and Leclerc 2004). We calculate the footprint area using model proposed by Kljun et al. (2015) for two wind direction ranges described in Sects. 4.2.1 and 4.2.2 for different stratification conditions (Fig. 8) at 19 m.

In stable stratification, the footprint is larger than in the unstable case. However, all footprint areas consist not only clearing near the mast, but also large roughness elements linked with the urban landscape. When the wind blows through tall trees (wind direction is from 140 to 250°) almost the entire contribution to the measured moments is made by the area with

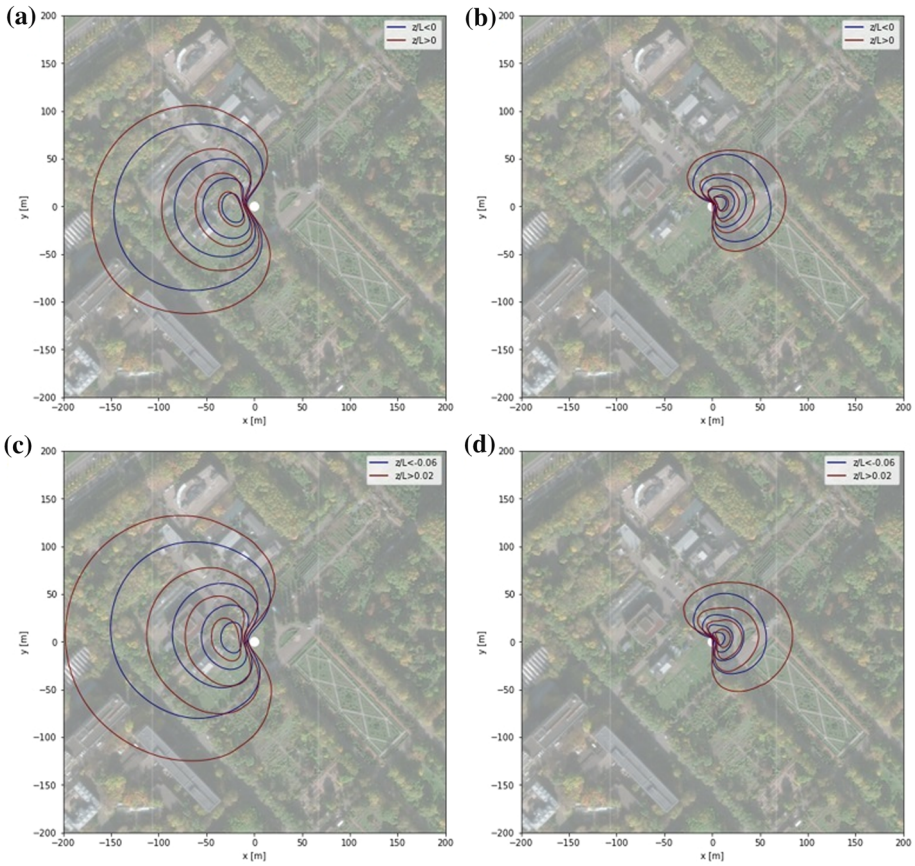

Fig. 8 Footprint area at level 19 m for wind directions from 0 to 100° (**a**, **c**) and 140° to 250° (**b**, **d**) under different stratification conditions. Red lines represent stable stratification and blue lines represent unstable case. Isolines represent 10, 30, 50 and 70% covering

tall trees. When the wind direction is from 0 to 100° small buildings and bushes contribute to the footprint area.

4.2.4 Relationships Between Second and Third Moments

Next, we consider how the constant C from Eq. (4) depends on the wind direction in this particular landscape. We consider all cases with $\zeta < 0$ and separately only more unstable cases with $\zeta < -0.06$, all cases with $\zeta > 0$ and separately only more stable cases with $\zeta > 0.02$.

When $\zeta < 0$, the coefficient C has large scatter and mostly has a positive value from 0 to 5 for all levels (Fig. 9a). While instability increases (Fig. 9b), the scattering of data decreases and constant C tends to the value $C = 2$ (as for a homogeneous surface) independent of the wind direction at 19 m, and for wind directions 0°–100° at 11 m, when this level is higher than the roughness elements. For $\zeta > 0$, the influence of the wind direction as well as the scattering of data within particular wind direction decreases as stability increases. Uncertainty of C decreases with increasing of the measurement level. The dimensionless third moment $\overline{w'w'T'}/u_* u_* T_*$ as a function of product $S_w\ \sigma_w/u_*$ for the wind direction range from 0 to 100° under unstable and stable stratification is shown in Fig. 10.

There is large scattering of data in the near-neutral cases at all levels (blue dots) for both stable and unstable cases. At levels 19 m and 11 m observations collapse into a straight line with increasing of instability (Fig. 10 a, b: scattering of red dots is less than of the blue ones) with a high correlation between $\overline{w'w'T'}/u_* u_* T_*$ and the product $S_w\ \sigma_w/u_*$ for

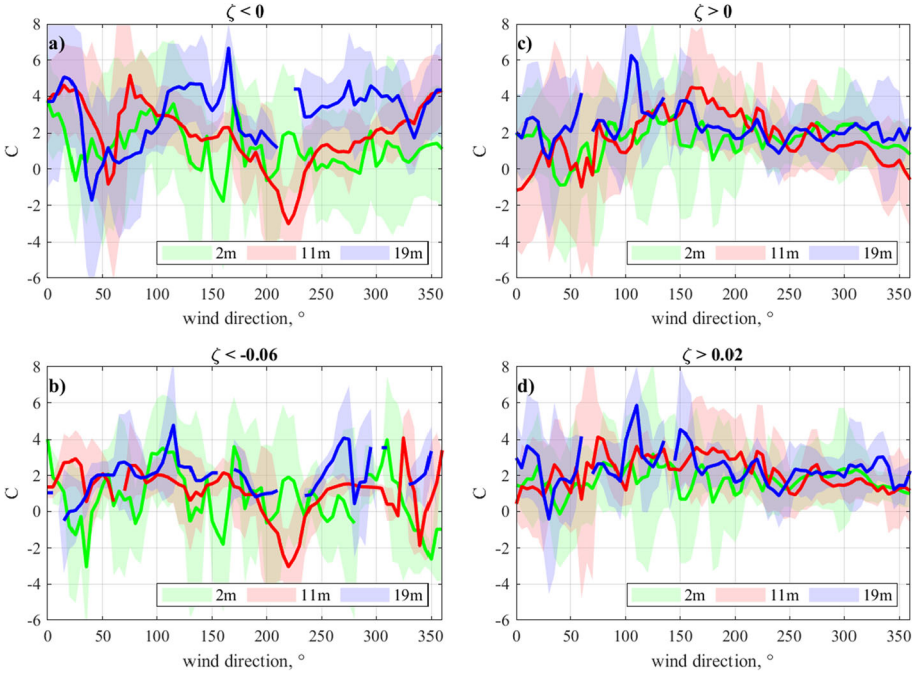

Fig. 9 Constant C as a function of wind direction. Lines mean average values and filled areas denote the plus/minus standard deviation

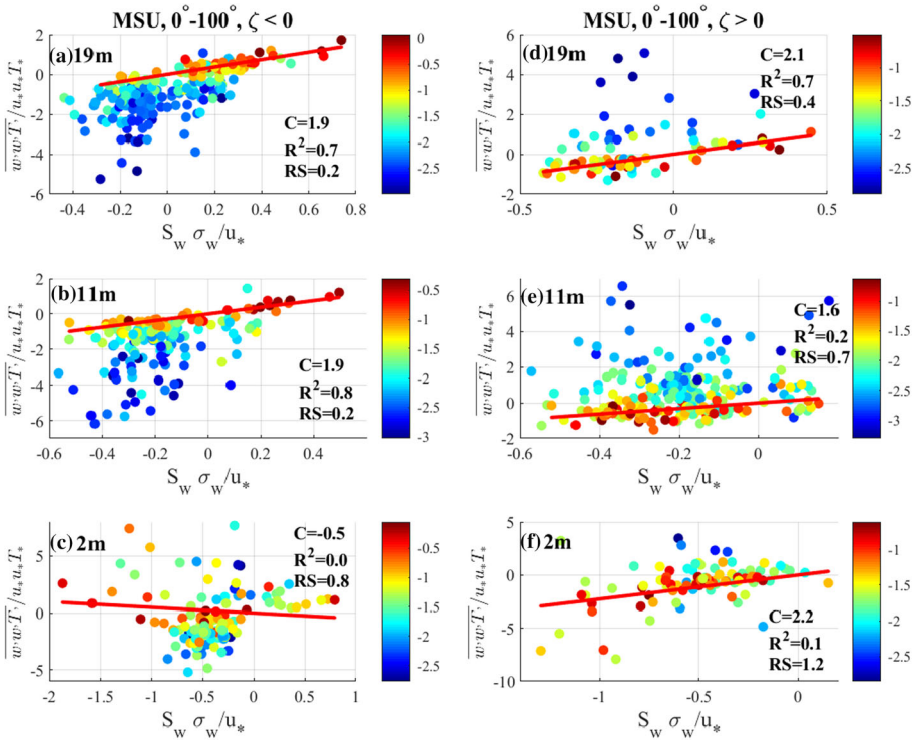

Fig. 10 Nondimensional third-order moment as a function of the product of skewness and standard deviation in cases of unstable (left column), and stable stratification (right column) at the levels of 19 m (**a**, **d**), 11 m (**b**, **e**) and 2 m (**c**, **f**) according to the MSU observations for the wind direction 0–100°. The dots denote observational data, and the red lines represent linear fit found by the least-squares method with $\zeta < -0.06$ for the left column and $\zeta > 0.02$ for right column. The colours of dots and the corresponding colorbars indicate the values of $\log_{10}\zeta$ and $\log_{10}(-\zeta)$ for stable and unstable states respectively

unstable stratification. The obtained values of the constant $C = 1.9$, of the coefficient of determination $R^2 = 0.7 - 0.8$, and of the relative scattering $RS = 0.2$ are equal or very close to results over flat surface at levels 30 m and 10 m under unstable conditions (Fig. 3 a,b). This shows that inhomogeneity of the landscape doesn't significantly affect the relationships between second and third moments in the CBL. It is interesting to note that in stable cases at levels 19 m and 11 m (Fig. 10d, e), while stability increases, the spread of the data decreases and the observations collapse into a straight line too. There is a good correlation between $\overline{w'w'T'}/u_*u_*T_*$ and the product $S_w\ \sigma_w/u_*$ for stable stratification at level 19 m: $R^2 = 0.7$ and slope $C = 2.1$, but relative scattering RS of data is larger in comparison to homogeneous case. Thus, stability reduces the influence of inhomogeneity at higher levels. There is almost no correlation between $\overline{w'w'T'}/u_*u_*T_*$ and the product $S_w\ \sigma_w/u_*$ independent of stability at level 2 m and in stable case at 11 m (Fig. 10c, e, f). The nondimensional third-order moment $\overline{w'w'T'}/u_*u_*T_*$ as a function of the product $S_w\ \sigma_w/u_*$ for the wind direction range from 140 to 250° under unstable and stable stratification is shown in Fig. 11. For this wind direction, the relationship between the second and third moments are generally the same as for the direction 0–100°, despite the fact that in this case the trees strongly distort the third moments

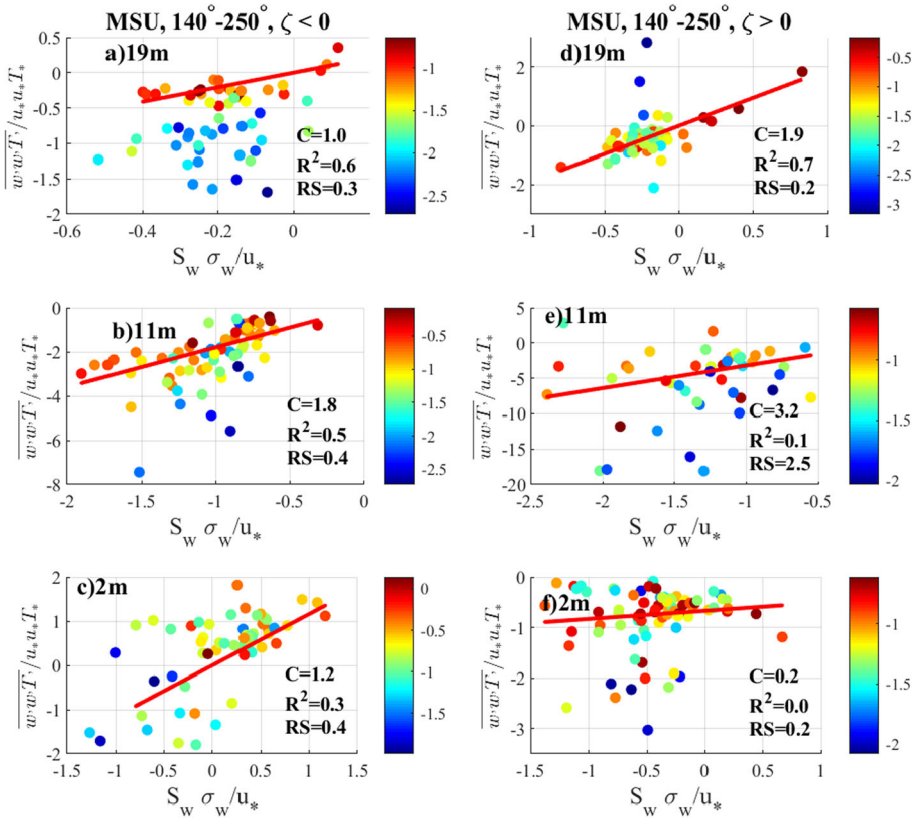

Fig. 11 As for Fig. 10, but for the for the wind direction 140–250°

themselves, as was described in the Sect. 4.2.2. The main difference with case 0–100° is that slope C at 19 m under unstable stratification (Fig. 11a) is twice as small.

4.3 Assessment of self-Correlation

A comparison of all observations as well as of the results of the self-correlation assessment is shown in Table 1. Intervals for each coefficient x_{rand} for random sets imply the intervals $[x_{\text{rand}} - \text{std}(x); x_{\text{rand}} + \text{std}(x)]$.

The coefficient of determination $R^2 \leq 0.2$ for all random sets. All observations with $R^2 > 0.2$ cannot be explained by self-correlation and must have a physical reason. Coefficient $C = 1.4 - 4.4$ for unstable cases on random sets, which is explained by the fact that all turbulent moments in this case take positive values. At the same time, for stable cases, the measurement data give a coefficient close to 2, while the random set gives values $C = 0.1 - 0.6$.

Table 1 All results and the results of self-correlation assessment

Site	Level	State	C	R^2	RS
Tsimlyansk	30 m	$\zeta < 0$	2.0	0.8	0.2
		$\zeta > 0$	1.6	0.7	0.2
	10 m	$\zeta < 0$	2.3	0.7	0.2
		$\zeta > 0$	1.8	0.6	0.3
	2 m	$\zeta < 0$	2.2	0.6	0.2
		$\zeta > 0$	1.0	0.3	0.4
MSU, 0–100°	19 m	$\zeta < 0$	1.9	0.7	0.2
		$\zeta > 0$	2.1	0.7	0.4
	10 m	$\zeta < 0$	1.9	0.8	0.2
		$\zeta > 0$	1.6	0.2	0.7
	2 m	$\zeta < 0$	− 0.5	0.0	0.8
		$\zeta > 0$	2.2	0.1	1.2
MSU, 140–250°	19 m	$\zeta < 0$	1.0	0.6	0.3
		$\zeta > 0$	1.9	0.7	0.2
	10 m	$\zeta < 0$	1.8	0.5	0.4
		$\zeta > 0$	3.2	0.1	2.5
	2 m	$\zeta < 0$	1.2	0.3	0.4
		$\zeta > 0$	0.2	0.0	0.2
Random sets from Tsimlyansk data	30 m	$\zeta < 0$	2.2–3.0	0.09–0.15	0.5–1.0
		$\zeta > 0$	0.3–0.6	0.15–0.20	0.08–0.16
	10 m	$\zeta < 0$	3.2–4.4	0.08–0.15	0.7–1.6
		$\zeta > 0$	0.1–0.3	0.11–0.15	0.03–0.07
	2 m	$\zeta < 0$	1.4–3.1	0.03–0.11	0.3–1.8
		$\zeta > 0$	− 0.4–0.1	0.00–0.05	0.06–0.18

5 Conclusions

We studied the relationships between second- and third-order moments under different stratification conditions over two types of contrasting landscapes—flat grassland and urban terrain. Over flat grassland, non-dimensional turbulent moments up to the third-order ones obey MOST. Specifically, the third-order moment $\overline{w'w'T'}/u_*u_*T_*$ increases for increasing instability. This reflects an increasing role of the nonlocal turbulent transport of heat flux due to convective motions. In this case, the relationship between the third- and second-order moments obtained using the framework of the mass-flux approach might be applicable. Namely, while instability increases both third moments $\overline{w'w'T'}/u_*u_*T_*$ and $S_w \frac{\sigma_w}{u_*}$ increase with a high correlation between both at all observational levels, but the coefficient of determination is larger at higher levels (30 m and 10 m) than close to the surface (2 m).

In stable conditions, the third-order moment $\overline{w'w'T'}/u_*u_*T_*$ is positive and does not demonstrate an explicit dependence onζ. At the same time, S_w decreases and changes sign from positive to negative as stability increases. Such a turbulent transport of heat flux might be associated with large eddies and sweep motions transporting downwards the heat flux

originating near the top of a stable ABL. As known from previous studies (e.g. Sun et al. 2012; Yus-Diez et al. 2019), such top-down turbulent events are associated with low-level jets or Kelvin—Helmholtz waves in the presence of a temperature inversion near the ABL top. Negative values of S_w were observed in such cases. Such a downward transport of negative heat flux by large eddies might explain the obtained correlation between $\overline{w'w'T'}/u_*u_*T_*$ and $S_w\ \sigma_w/u_*$, making applicable the mass-flux approach even in the stable boundary layer at levels 30 m and partly at 10 m. However, further analysis is needed to prove this hypothesis including quadrant analysis and other methods of detecting coherent structures.

Observations over complex urban terrain display differences in comparison to flat grassland under neutral stratification. When the flow passes over small buildings, bushes etc., nondimensional turbulent moments at higher observational levels do not significantly differ from those over flat surface. This suggests that higher levels significantly exceed the typical height of roughness elements. At levels whose height is of the same order as the height of roughness elements σ_w/u_* increases and S_w becomes negative. Such a behaviour is known for urban and forest canopies. Moreover, the height of the increased magnitude of these moments is found to correlate with the height of the upwind roughness elements. Despite the similarities of the obtained results to the known features of a canopy sublayer, our data suggests that the increased values of σ_w/u_*, S_w and $\overline{w'w'T'}/u_*u_*T_*$ are shifted closer towards the ground. This points to a possible important role of turbulent transport due to large eddies at that height.

For levels above inhomogeneity, the mass-flux approach is applicable while the instability increases. Thus, correlation between the second- and third-order moments does not depend on landscape features. Furthermore, the relationship obtained in the framework of the mass-flux approach holds also under stable conditions at levels 19 m and 11 m.

To conclude, our study documented deviations of selected turbulence statistics from the classical universal functions. The analysis of the third-order moments reveals that the nonlocal transport due to large eddies might play an important role especially within an urban canopy and has to be included in turbulence closures. Earth system models and mesoscale models employ increasingly complex parametrizations for the ABL, requiring surface boundary conditions for numerous higher order turbulence statistics, such as the turbulent kinetic energy flux, temperature dispersion flux, etc. Typically such boundary conditions are obtained from the surface-layer parametrization based on MOST. However, heterogeneous landscapes represent conditions where the assumptions of MOST might not be valid and MOST has to be adjusted or extended. Our study shows that indeed the deviations from the classical universal functions used within MOST are especially pronounced over the heterogeneous urban landscape.

As a possible pathway to tackle this problem we explored the applicability over different landscapes of a relation between the third-order turbulent transport of heat flux and the vertical velocity skewness and variance which was originally obtained for the CBL within a mass-flux approach. Such an approach is especially useful in conditions where a local similarity does not hold. Here we show that such an approach might also be useful over a heterogeneous urban landscape and might be used to further improve urban canopy models. However such a hypothesis requires further data analysis focusing also on the momentum transfer which represents a prospect of a future work.

Acknowledgements This study is largely based on the ideas of Sergey Zilitinkevich. His works as well as personal discussions with him motivated and inspired authors of this research. Collection and analysis of the measurement data were supported by Russian Science Foundation, Grant 21-17-00249; the partial processing of turbulent data was supported by Russian Foundation of Basic Research, grant 20-05-00834; the

measurements and pre-processing in MSU was supported by the Ministry of Science and Higher Education of Russia (Agreements 075-15-2021-574) and as part of the program of the Moscow Center for Fundamental and Applied Mathematics under the agreement № 075-15-2022-284. Carrying out of the Tsimlyansk experiment was supported by the Russian Science Foundation grant 18-77-10072-P.

Data Availability The datasets generated and analysed during the current study are available in the b2share.eudat.eu repository, [https://b2share.eudat.eu/records/ba2a9eb8f6d94a8eb4145c7f772be633].

Declarations

Conflicts of interest The authors declare no conflict of interest.

References

Abdella K, McFarlane N (1997) A new second-order turbulence closure scheme for the planetary boundary layer. J Atmos Sci 54:1850–1867

Abdella K, McFarlane N (1999) NOTES AND CORRESPONDENCE-reply-comments on a new second-order turbulence closure scheme for the planetary boundary layer. J Atmos Sci 56:3482–3483

Abdella K, Petersen AC (2000) Third-order moment closure through a mass-flux approach. Boundary-Layer Meteorol 95(2):303–318

Ala-Könni J, Kohonen KM, Leppäranta M, Mammarella I (2021) Validation of turbulent heat transfer models against eddy covariance flux measurements over a seasonally ice covered lake. Geosci Model Dev Discussions: 1–23

Ament F, Simmer C (2006) Improved representation of land-surface heterogeneity in a non-hydrostatic numerical weather prediction model. Boundary-Layer Meteorol 121(1):153–174

Andreas EL, Hill RJ, Gosz JR, Moore DI, Otto WD, Sarma AD (1998) Statistics of surface-layer turbulence over terrain with metre-scale heterogeneity. Boundary-Layer Meteorol 86(3):379–408

Ariel NZ, Nadezhina E (1977) Dimensionless turbulence characteristics under various stratification conditions (in ground-level atmospheric layer). Izv Atmos Ocean Phys 12:492–497

Babić K, Rotach MW, Klaić ZB (2016a) Evaluation of local similarity theory in the wintertime nocturnal boundary layer over heterogeneous surface. Agric for Meteorol 228:164–179

Babić N, Večenaj Ž, De Wekker SF (2016b) Flux–variance similarity in complex terrain and its sensitivity to different methods of treating non-stationarity. Boundary-Layer Meteorol 159(1):123–145

Banerjee T, De Roo F, Mauder M (2017) Connecting the failure of K theory inside and above vegetation canopies and ejection–sweep cycles by a large-eddy simulation. J Appl Meteorol Climatol 56(12):3119–3131

Barskov KV, Chernyshev RV, Stepanenko VM, Repina IA, Artamonov AY, Guseva SP, Gavrikov AV (2017) Experimental study of heat and momentum exchange between a forest lake and the atmosphere in winter. IOP Conf Ser Earth Environ Sci 96:012003

Barskov KV, Glazunov AV, Repina IA, Stepanenko VM, Lykossov VN, Mammarella I (2018) On the applicability of similarity theory for the stable atmospheric boundary layer over complex terrain. Izv Atmos Ocean Phys 54(5):462–471

Barskov K, Stepanenko V, Repina I, Artamonov A, Gavrikov A (2019) Two regimes of turbulent fluxes above a frozen small lake surrounded by forest. Boundary-Layer Meteorol 173(3):311–320

Boehrer B, Schultze M (2008) Stratification of lakes. J Geophys Res. https://doi.org/10.1029/2006RG000210

Bou-Zeid E, Meneveau C, Parlange MB (2004) Large-eddy simulation of neutral atmospheric boundary layer flow over heterogeneous surfaces: blending height and effective surface roughness. Water Resour Res. https://doi.org/10.1029/2003WR002475

Bou-Zeid E, Anderson W, Katul GG, Mahrt L (2020) The persistent challenge of surface heterogeneity in boundary-layer meteorology: a review. Boundary-Layer Meteorol 177(2):227–245

Caughey SJ, Wyngaard JC, Kaimal JC (1979) Turbulence in the evolving stable boundary layer. J Atmos Sci 36(6):1041–1052

Cava D, Katul GG, Scrimieri A, Poggi D, Cescatti A, Giostra U (2006) Buoyancy and the sensible heat flux budget within dense canopies. Boundary-Layer Meteorol 118(1):217–240

Chiba O (1978) Stability dependence of the vertical wind velocity skewness in the atmospheric surface layer. J Meteorol Soc Jpn Ser II 56(2):140–142

Condie SA, Webster IT (2001) Estimating stratification in shallow water bodies from mean meteorological conditions. J Hydraul Eng 127(4):286–292
De Bruin HAR, Kohsiek W, Van Den Hurk BJJM (1993) A verification of some methods to determine the fluxes of momentum, sensible heat, and water vapour using standard deviation and structure parameter of scalar meteorological quantities. Boundary-Layer Meteorol 63(3):231–257
Dellwik E, Jensen NO (2005) Flux–profile relationships over a fetch limited beech forest. Boundary-Layer Meteorol 115(2):179–204
Denmead OT, Bradley EF (1985) Flux-gradient relationships in a forest canopy the Forest-Atmosphere Interaction. Springer, Dordrecht, pp 421–442
Dias NL, Brutsaert W, Wesely ML (1995) Z-less stratification under stable conditions. Boundary-Layer Meteorol 75(1):175–187
Dupont S, Brunet Y (2009) Coherent structures in canopy edge flow: a large-eddy simulation study. J Fluid Mech 630:93–128
Ferrero E (2005) Third-order moments for shear driven boundary layer. Boundary-Layer Meteorol 116(3):461–466
Finnigan J (2000) Turbulence in plant canopies. Annu Rev Fluid Mech 32(1):519–571
Finnigan JJ, Shaw RH, Patton EG (2009) Turbulence structure above a vegetation canopy. J Fluid Mech 637:387–424
Foken T (2017) Micrometeorology. Springer, Berlin, Heidelberg, p 362
Foken T, Leclerc MY (2004) Methods and limitations in validation of footprint models. Agric for Meteorol 127:223–234
Foken T, Wichura B (1996) Tools for quality assessment of surface-based flux measurements. Agric for Meteorol 78(1–2):83–105
Foken T, Skeib G, Richter SH (1991) Dependence of the integral turbulence characteristics on the stability of stratification and their use for Doppler-Sodar measurements. Z Meteorol 41:311–315
Fontan S, Katul G, Poggi D, Manes C, Ridolfi L (2013) Flume experiments on turbulent flows across gaps of permeable and impermeable boundaries. Boundary-Layer Meteorol 147(1):21–39
Garratt JR (1990) The internal boundary layer—a review. Boundary-Layer Meteorol 50(1–4):171–203
Giorgi F, Avissar R (1997) Representation of heterogeneity effects in earth system modeling: experience from land surface modeling. Rev Geophys 35(4):413–437
Glazunov AV, Stepanenko VM (2015) Large-eddy simulation of stratified turbulent flows over heterogeneous landscapes. Izv Atmos Ocean Phys 51(4):351–361
Göckede M, Rebmann C, Foken T (2004) A combination of quality assessment tools for eddy covariance measurements with footprint modelling for the characterisation of complex sites. Agric for Meteorol 127(3–4):175–188
Grachev AA, Andreas EL, Fairall CW, Guest PS, Persson POG (2013) The critical Richardson number and limits of applicability of local similarity theory in the stable boundary layer. Boundary-Layer Meteorol 147(1):51–82
Grachev AA, Andreas EL, Fairall CW, Guest PS, Persson POG (2015) Similarity theory based on the Dougherty-Ozmidov length scale. Q J R Meteorol Soc 141(690):1845–1856
Grachev AA, Leo LS, Fernando HJ, Fairall CW, Creegan E, Blomquist BW, Hocut CM (2018) Air–sea/land interaction in the coastal zone. Boundary-Layer Meteorol 167(2):181–210
Gryanik VM, Hartmann J (2002) A turbulence closure for the convective boundary layer based on a two-scale mass-flux approach. J Atmos Sci 59(18):2729–2744
Hicks BB (1981) An examination of turbulence statistics in the surface boundary layer. Boundary-Layer Meteorol 21(3):389–402
Hicks BB (1978) Some limitations of dimensional analysis and power laws. Boundary-Layer Meteorol (Netherlands) 14.
Higgins CW, Pardyjak E, Froidevaux M, Simeonov V, Parlange MB (2013) Measured and estimated water vapor advection in the atmospheric surface layer. J Hydrometeorol 14(6):1966–1972
Izumi Y (1971) Kansas 1968 field program data report (No. 379). Air Force Cambridge Research Laboratories, Air Force Systems Command, United States Air Force
Jacobs AF, van de Wiel BJ, Holtslag AA (2001) Daily course of skewness and kurtosis within and above a crop canopy. Agric for Meteorol 110(2):71–84
Kader BA, Yaglom AM (1990) Mean fields and fluctuation moments in unstably stratified turbulent boundary layers. J Fluid Mech 212:637–662
Kaimal JC, Finnigan JJ (1994) Atmospheric boundary layer flows: their structure and measurements. Oxford University Press, Oxford
Katul GG, Cava D, Siqueira M, Poggi D (2013) Scalar turbulence within the canopy sublayer. Coherent Flow Struct Earth's Surf. https://doi.org/10.1002/9781118527221.ch6

Kenny WT, Bohrer G, Morin TH, Vogel CS, Matheny AM, Desai AR (2017) A numerical case study of the implications of secondary circulations to the interpretation of eddy-covariance measurements over small lakes. Boundary-Layer Meteorol 165(2):311–332
Klipp CL, Mahrt L (2004) Flux-gradient relationship, self-correlation and intermittency in the stable boundary layer. Q J R Meteorol Soc 130:2087–2103
Kljun N, Calanca P, Rotach MW, Schmid HP (2015) A simple two-dimensional parameterisation for Flux Footprint Prediction (FFP). Geosci Model Dev 8(11):3695–3713
Kral ST, Sjöblom A, Nygård T (2014) Observations of summer turbulent surface fluxes in a High Arctic fjord. Q J R Meteorol Soc 140(679):666–675
Lumley JL, Panofsky HA (1964) The structure of atmospheric turbulence. Interscience Publishers, New York, p 239
Lyu R, Hu F, Liu L, Xu J, Cheng X (2018) High-order statistics of temperature fluctuations in an unstable atmospheric surface layer over grassland. Adv Atmos Sci 35(10):1265–1276
Mahrt L (2010) Computing turbulent fluxes near the surface: Needed improvements. Agric for Meteorol 150(4):501–509
Markfort CD, Perez AL, Thill JW, Jaster DA, Porté-Agel F, Stefan HG (2010) Wind sheltering of a lake by a tree canopy or bluff topography. Water Resour Res. https://doi.org/10.1029/2009WR007759
Maurizi A, Robins A (2000) Boundary-layer flow and dispersion over a two-dimensional hill; high-order statistics of the flow and concentration fields, experiment performed at EnFlo, UniSurrey, UK.
Maurizi A, Tampieri F (2013) Some considerations on skewness and kurtosis of vertical velocity in the convective boundary layer. arXiv preprint arXiv:1310.4321
McBean GA (1971) The variation of the statistics of wind, temperature and humidity fluctuations with stability. Boundary-Layer Meteorol 1:438–457
Medjnoun T, Vanderwel C, Ganapathisubramani B (2018) Characteristics of turbulent boundary layers over smooth surfaces with spanwise heterogeneities. J Fluid Mech 838:516–543
Michaelis J, Lüpkes C, Zhou X, Gryschka M, Gryanik VM (2020) Influence of lead width on the turbulent flow over sea ice leads: modeling and parametrization. J Geophys Res Atmos 125(15):e2019JD031996
Mironov DV, Gryanik VM, Lykossov VN, Zilitinkevich SS (1999) Comments on "A new second-order turbulence closure scheme for the planetary boundary layer." J Atmos Sci 56(19):3478–3481
Mironov DV, Gryanik VM, Moeng CH, Olbers DJ, Warncke TH (2000) Vertical turbulence structure and second-moment budgets in convection with rotation: A large-eddy simulation study. Q J R Meteorol Soc 126(563):477–515
Moeng CH, Rotunno R (1990) Vertical velocity skewness in the buoyancy driven boundary layer. J Atmos Sci 47:1149–1162
Monin AS, Obukhov AM (1954) Basic laws of turbulent mixing in the surface layer of the atmosphere. Contrib Geophys Inst Acad Sci USSR 151(163):e187
Monin AS, Yaglom AM (1971) Statistical fluid mechanics: mechanics of turbulence, vol 1. MIT Press, Cambridge, MA, p 462
Monin AS, Yaglom AM (1992) Statistical fluid dynamics, vol 1. Gidrometeoizdat, St. Petersburg
Moraes OL, Acevedo OC, Degrazia GA, Anfossi D, da Silva R, Anabor V (2005) Surface layer turbulence parameters over a complex terrain. Atmos Environ 39(17):3103–3112
Mordukhovich MI, Tsvang LR (1966) Direct measurements of turbulent flows at two elevations in the atmospheric surface layer (Atmospheric turbulence statistical characteristics dependence on stratification and elevation from heat flux and wind friction stress characteristics). Izv Atmos Ocean Phys 2:786–803
Nakamura R, Mahrt L (2001) Similarity theory for local and spatially averaged momentum fluxes. Agric for Meteorol 108(4):265–279
Obukhov AM (1946) Turbulence in an atmosphere with a non-uniform temperature. Trudy Inst Teoret Geofiz Akad Nauk SSSR 1:95–115 (translation in: (1971) Boundary-Layer Meteorol 2: 7–29)
Panofsky HA, Dutton JA (1984) Atmospheric turbulence-models and methods for engineering applications. John Wiley and Sons, New York, p 397
Panofsky HA, Tennekes H, Lenschow DH, Wyngaard JC (1977) The characteristics of turbulent velocity components in the surface layer under convective conditions. Boundary-Layer Meteorol 11:355–361
Patton EG, Sullivan PP, Shaw RH, Finnigan JJ, Weil JC (2016) Atmospheric stability influences on coupled boundary layer and canopy turbulence. J Atmos Sci 73(4):1621–1647
Poggi D, Katul GG, Albertson JD (2004) Momentum transfer and turbulent kinetic energy budgets within a dense model canopy. Boundary-Layer Meteorol 111(3):589–614
Quan L, Hu F (2009) Relationship between turbulent flux and variance in the urban canopy. Meteorol Atmos Phys 104(1):29–36
Quan L, Ferrero E, Hu F (2012) Relating statistical moments and entropy in the stable boundary layer. Physica A Stat Mech Appl 391(1–2):231–247

Raasch S, Harbusch G (2001) An analysis of secondary circulations and their effects caused by small-scale surface inhomogeneities using large-eddy simulation. Boundary-Layer Meteorol 101(1):31–59
Randall DA, Shao Q, Moeng CH (1992) A second-order bulk boundary-layer model. J Atmos Sci 49(20):1903–1923
Rao KS, Wyngaard JC, Coté OR (1974) Local advection of momentum, heat, and moisture in micrometeorology. Boundary-Layer Meteorol 7(3):331–348
Raupach MR (1989) Applying Lagrangian fluid mechanics to infer scalar source distributions from concentration profiles in plant canopies. Agric for Meteorol 47(2–4):85–108
Raupach MR, Coppin PA, Legg BJ (1986) Experiments on scalar dispersion within a model plant canopy part I: the turbulence structure. Boundary-Layer Meteorol 35(1):21–52
Ris RC, Holthuijsen LH, Booij N (1999) A third-generation wave model for coastal regions: 2 Verification. J Geophys Res Oceans 104(C4):7667–7681
Rodrigo JS, Anderson PS (2013) Investigation of the stable atmospheric boundary layer at Halley Antarctica. Boundary-Layer Meteorol 148(3):517–539
Seginer I, Mulhearn PJ, Bradley EF, Finnigan JJ (1976) Turbulent flow in a model plant canopy. Boundary-Layer Meteorol 10(4):423–453
Sodemann H, Foken T (2004) Empirical evaluation of an extended similarity theory for the stably stratified atmospheric surface layer. Q J R Meteorol Soc 130:2665–2671
Sodemann H, Foken T (2005) Special characteristics of the temperature structure near the surface. Theor Appl Climatol 80(2):81–89
Soloviev YP, Kudryavtsev VN (2010) Wind-speed undulations over swell: field experiment and interpretation. Boundary-Layer Meteorol 136(3):341–363
Sorbjan Z (1989) Structure of the atmospheric boundary layer (No. 551.51 SOR)
Sreenivasan KR, Chambers AJ, Antonia RA (1978) Accuracy of moments of velocity and scalar fluctuations in the atmospheric surface layer. Boundary-Layer Meteorol 14(3):341–359
Stull RB (1988) An introduction to boundary layer meteorology, Vol 13, Springer Science & Business Media.
Sun J, Mahrt L, Banta RM, Pichugina YL (2012) Turbulence regimes and turbulence intermittency in the stable boundary layer during CASES-99. J Atmos Sci 69(1):338–351
Sun J, Lenschow DH, LeMone MA, Mahrt L (2016) The role of largecoherent-eddy transport in the atmospheric surface layer based on CASES-99 observations. Boundary-Layer Meteorol 160(1):83–111
Tsvang LR, Koprov BM, Zubkovskij SL, Dyer AJ, Hicks BB, Miyake M, Stewart RW, McDonald JW (1973) Comparison of turbulence measurements by different instuments; tsimlyansk field experiment 1970. Boundary-Layer Meteorol 3:499–521
Tsvang LR, Zubkovskij SL, Kader BA, Kallistratova MA, Foken T, Gerstmann W, Przandka Z, Pretel J, Zelenry J, Keder J (1985) International turbulence comparison experiment (ITCE-81). Boundary-Layer Meteorol 31:325–348
Wilson NR, Shaw RH (1977) A higher order closure model for canopy flow. J Appl Meteorol 16(11):1197–1205
Wood CR, Lacser A, Barlow JF, Padhra A, Belcher SE, Nemitz E, Grimmond CSB (2010) Turbulent flow at 190 m height above London during 2006–2008: a climatology and the applicability of similarity theory. Boundary-Layer Meteorol 137(1):77–96
Wyngaard JC (1973) On surface-layer turbulence. In: Haugen DA (ed) Workshop on micrometeorology. American Meteorology Society, Boston, pp 101–149
Wyngaard JC (2010) Turbulence in the atmosphere. Cambridge University Press
Wyngaard JC, Coté OR, Izumi Y (1971) Local free convection, similarity, and the budgets of shear stress and heat flux. J Atmos Sci 28(7):1171–1182
Yus-Díez J, Udina M, Soler MR, Lothon M, Nilsson E, Bech J, Sun J (2019) Nocturnal boundary layer turbulence regimes analysis during the BLLAST campaign. Atmos Chem Phy 19(14):9495–9514
Zaitseva DV, Kallistratova MA, Lyulyukin VS, Kouznetsov RD, Kuznetsov DD (2018) The effect of internal gravity waves on fluctuations in meteorological parameters of the atmospheric boundary layer. Izv Atmos Ocean Phys 54(2):173–181
Zhao Z, Gao Z, Li D, Bi X, Liu C, Liao F (2013) Scalar flux–gradient relationships under unstable conditions over water in coastal regions. Boundary-Layer Meteorol 148(3):495–516
Zilitinkevich SS (2002) Third-order transport due to internal waves and non-local turbulence in the stably stratified surface layer. Q J R Meteorol Soc J Atmosp Sci Appl Meteorol Phys Oceanogr 128(581):913–925
Zilitinkevich S, Grachev A, Hunt JCR (1998) Surface frictional processes and non-local heat/mass transfer in the shear-free convective boundary layer Buoyant convection in geophysical flows. Springer, Dordrecht, pp 83–113
Zilitinkevich S, Gryanik VM, Lykossov VN, Mironov DV (1999) Third-order transport and nonlocal turbulence closures for convective boundary layers. J Atmos Sci 56:3463–3477

Zilitinkevich SS, Hunt JCR, Esau IN, Grachev AA, Lalas DP, Akylas E, Joffre SM (2006) The influence of large convective eddies on the surface-layer turbulence. Q J R Meteorol Soc J Atmosp Sci Appl Meteorol Phys Oceanogr 132(618):1426–1456

Zilitinkevich S, Kadantsev E, Repina I, Mortikov E, Glazunov A (2021) Order out of chaos: Shifting paradigm of convective turbulence. J Atmos Sci 78(12):3925–3932

Terms and Conditions

Springer Nature journal content, brought to you courtesy of Springer Nature Customer Service Center GmbH ("Springer Nature").

Springer Nature supports a reasonable amount of sharing of research papers by authors, subscribers and authorised users ("Users"), for small-scale personal, non-commercial use provided that all copyright, trade and service marks and other proprietary notices are maintained. By accessing, sharing, receiving or otherwise using the Springer Nature journal content you agree to these terms of use ("Terms"). For these purposes, Springer Nature considers academic use (by researchers and students) to be non-commercial.

These Terms are supplementary and will apply in addition to any applicable website terms and conditions, a relevant site licence or a personal subscription. These Terms will prevail over any conflict or ambiguity with regards to the relevant terms, a site licence or a personal subscription (to the extent of the conflict or ambiguity only). For Creative Commons-licensed articles, the terms of the Creative Commons license used will apply.

We collect and use personal data to provide access to the Springer Nature journal content. We may also use these personal data internally within ResearchGate and Springer Nature and as agreed share it, in an anonymised way, for purposes of tracking, analysis and reporting. We will not otherwise disclose your personal data outside the ResearchGate or the Springer Nature group of companies unless we have your permission as detailed in the Privacy Policy.

While Users may use the Springer Nature journal content for small scale, personal non-commercial use, it is important to note that Users may not:

1. use such content for the purpose of providing other users with access on a regular or large scale basis or as a means to circumvent access control;
2. use such content where to do so would be considered a criminal or statutory offence in any jurisdiction, or gives rise to civil liability, or is otherwise unlawful;
3. falsely or misleadingly imply or suggest endorsement, approval , sponsorship, or association unless explicitly agreed to by Springer Nature in writing;
4. use bots or other automated methods to access the content or redirect messages
5. override any security feature or exclusionary protocol; or
6. share the content in order to create substitute for Springer Nature products or services or a systematic database of Springer Nature journal content.

In line with the restriction against commercial use, Springer Nature does not permit the creation of a product or service that creates revenue, royalties, rent or income from our content or its inclusion as part of a paid for service or for other commercial gain. Springer Nature journal content cannot be used for inter-library loans and librarians may not upload Springer Nature journal content on a large scale into their, or any other, institutional repository.

These terms of use are reviewed regularly and may be amended at any time. Springer Nature is not obligated to publish any information or content on this website and may remove it or features or functionality at our sole discretion, at any time with or without notice. Springer Nature may revoke this licence to you at any time and remove access to any copies of the Springer Nature journal content which have been saved.

To the fullest extent permitted by law, Springer Nature makes no warranties, representations or guarantees to Users, either express or implied with respect to the Springer nature journal content and all parties disclaim and waive any implied warranties or warranties imposed by law, including merchantability or fitness for any particular purpose.

Please note that these rights do not automatically extend to content, data or other material published by Springer Nature that may be licensed from third parties.

If you would like to use or distribute our Springer Nature journal content to a wider audience or on a regular basis or in any other manner not expressly permitted by these Terms, please contact Springer Nature at

onlineservice@springernature.com